Title	Temperature-induced isostructural phase transition, associated large negative volume expansion, and the existence of a critical point in the phase diagram of the multiferroic (1-x)BiFeO3-xPbTiO3 solid solution system
Auther(s)	Bhattacharjee, Shuvrajyoti; Taji, Kazuaki; Moriyoshi, Chikako; Kuroiwa, Yoshihiro; Pandey, Dhananjai
Citation	Physical Review B , 84 (10) : 104116
Issue Date	2011
DOI	10.1103/PhysRevB.84.104116
Self DOI	
URL	http://ir.lib.hiroshima-u.ac.jp/00033895
Right	(c) 2011 American Physical Society
Relation	

Temperature-induced isostructural phase transition, associated large negative volume expansion, and the existence of a critical point in the phase diagram of the multiferroic (1–x)$BiFeO_3$–$x$$PbTiO_3$ solid solution system

Shuvrajyoti Bhattacharjee,[1] Kazuaki Taji,[2] Chikako Moriyoshi,[2] Yoshihiro Kuroiwa,[2] and Dhananjai Pandey[1,*]
[1]*School of Materials Science and Technology, Institute of Technology, Banaras Hindu University, Varanasi-221005, India*
[2]*Department of Physical Science, Graduate School of Science, Hiroshima University, Higashi-Hiroshima, Hiroshima 739-8526, Japan*
(Received 28 December 2010; revised manuscript received 14 June 2011; published 12 September 2011)

We report here an unusual ferroelectric to ferroelectric isostructural phase transition and associated giant negative thermal expansion (NTE) for the tetragonal composition $x = 0.31$ closest to the morphotropic phase boundary (MPB) of the multiferroic (1–x)$BiFeO_3$–$x$$PbTiO_3$ (BF-xPT) solid solution system. It is shown that the room temperature tetragonal phase (T_1) of BF-0.31PT with extremely large tetragonality undergoes a first-order isostructural phase transition to another tetragonal phase (T_2) with lower tetragonality without losing the $P4mm$ space group symmetry and the occupied Wyckoff positions. The T_2 phase finally transforms into the paraelectric cubic phase at still higher temperatures. Using group theoretical considerations, we show that the observed atomic displacements associated with this isostructural phase transition correspond to specific irreducible representations of the $P4mm$ space group at its Brillouin zone center, and as such this transition may be phonon driven. Pronounced anomalies in the thermal displacement parameters at the T_1 to T_2 transition provide evidence for such a phonon-mediated isostructural phase transition. The high tetragonality ferroelectric phase (T_1) of BF-0.31PT shows the largest NTE coefficient reported so far in the mixed BF-xPT system. The isostructural transition is shown to persist for tetragonal compositions of BF-xPT up to $x = 0.60$. A complete phase diagram of the BF-xPT system showing the existence of a critical point at $T \sim 677$ K for $x \approx 0.63$ is also presented.

DOI: 10.1103/PhysRevB.84.104116 PACS number(s): 77.80.B−

I. INTRODUCTION

A structural phase transition in a crystalline material is marked with change in lattice symmetry as a function of temperature (T), pressure (P), or composition (x). Generally, some symmetry element of the parent high symmetry phase is lost at the phase transition temperature (T_C), pressure (P_C), or composition (x_C) and the lost symmetry determines the nature of order parameter characterizing a second-order phase transition.[1] As a result, the transformed phase has lower symmetry. Important exceptions, like those in reconstructive first-order phase transitions, in which transformed phase has a higher symmetry, are also known in nature.[2] In second-order phase transitions, the high and the low symmetry phases bear a group-subgroup relationship, and the order parameter corresponds to one of the irreducible representations (Irreps) of the high symmetry phase.[2,3] When the order parameter is coupled to the lattice strain, a potentially second-order phase transition may show first-order character as it happens in several ferroelectric perovskites like $BaTiO_3$, $PbTiO_3$, etc.[4] While structural phase transitions involving change of space group symmetry are ubiquitous in nature, there are also known examples of less commonly observed isostructural phase transitions which preserve the space group symmetry and the type of occupied Wyckoff positions. Such transitions manifest through sharp change of some macroscopic property of the system like volume, resistivity, etc.[5] In addition an isostructural phase transition may also exhibit sharp changes in the atomic positions consistent with the displacement pattern of one of the modes corresponding to an Irrep of the space group symmetry of the parent phase without changing the space group symmetry and the occupied Wyckoff positions. Isostructural phase transitions are somewhat uncommon, especially at ambient pressures, and have therefore always attracted much experimental and theoretical interest. The possibility of location of a critical point in the phase diagram of compounds showing isostructural phase transition makes the study of such transitions even more exciting.[5,6] A critical point can only exist for phases which do not differ in internal symmetry,[3] and hence systems exhibiting isostructural phase transition are ideal candidates for search for critical points. Experimentally, high pressure has generally been employed to study changes accompanying isostructural phase transitions using diffraction (x-ray and neutron diffraction) and resistivity measurement techniques.[6–8]

Isostructural phase transitions related to valence fluctuation phenomena under high pressures are well studied in several rare earth metals and their alloys/compounds. Most widely studied isostructural phase transition is the α-γ transition in Ce,[6,7] which undergoes a first-order isostructural phase transition from an antiferromagnetic, high-resistive γ form to a nonmagnetic, low-resistive α form, both having face-centered cubic structure ($Fm\bar{3}m$). This transition is accompanied with a 15% volume collapse at room temperature at a critical pressure of ∼0.7 GPa. The promotion of one 4f electron to the 5d level is considered to be the reason for this volume collapse,[6–8] although other alternative mechanisms have also been proposed to explain this phenomenon.[9] In the P-T phase diagram of Ce, there exists a critical point at high temperatures and pressures.[6] Many Ce-based compounds also show this type of isostructural phase transition.[10]

Among the inorganic compounds, tin chloride dihydrate ($SnCl_2 \cdot 2H_2O$) has been reported to undergo an order-disorder type isostructural phase transition at −57 °C under ambient pressure.[11,12] The order-disorder phase transition has been

ascribed to the ordering of hydrogen atoms within the layer of hydrogen-bonded water molecules.[11] This transition is accompanied with an anomaly in the dielectric constant, dc conductivity, and proton-resonance spectra without breaking the internal symmetry. In the case of antiferromagnetic inorganic compounds, the deformation in the arrangement of magnetic atoms existing above the antiferromagnetic Néel temperature is a natural consequence of the arrangement of adjacent magnetic atoms in antiparallel spin orientation below the transition temperature. This deformation in the crystal structure of antiferromagnetic compounds on passing through the magnetic transition temperature was investigated in the pioneering work in the early 1950s of the 20th century by Greenwald *et al.*[13] Recently, isostructural phase transitions occurring across antiferromagnetic transition in multiferroics have been shown to be responsible for the magnetoelectric coupling.[14,15]

An isostructural phase transition in the vicinity of a displacive ferroelectric-transition temperature between two isostructural ferroelectric phases is not well known. Using first principle calculations, several ABO_3 perovskites have been predicted to show anomalously large tetragonality under negative pressure[16] related to isostructural phase transition. Similarly, under the influence of stress induced by the substrate, thin films of $BiFeO_3$ (BF) were theoretically predicted to undergo an isostructural phase transition for the monoclinic *Cc* phase whose *c*/*a* ratio increases anomalously from ∼1.05 to ∼1.3 as a result of stress.[17] However, more recent reports suggest that with increase in strain the rhombohedral (R) phase of BF changes first to an R-like M_A phase (monoclinic) phase, then to tetragonal (T)-like M_C (monoclinic) phase without any evidence for the isostructural phase transition claimed previously.[17]

We report here an isostructural phase transition at high temperatures under ambient atmospheric pressure with a large discontinuous change in the tetragonality in bulk powders of the mixed multiferroic system $(1–x)BiFeO_3–xPbTiO_3$ (BF-*x*PT) with $x = 0.31$. This transition is shown to be of first-order character and is not linked with the magnetic transition, as in other multiferroics,[14,15] or valence fluctuations, as in several rare earth metals, their alloys, and compounds;[6,7] however, it is interestingly linked with two tetragonal phases (T_1 and T_2) of different tetragonalities, both of which are ferroelectric. The transition is accompanied with an unusually large volume collapse due to negative thermal expansion (NTE) of the tetragonal phase, which appears first below the ferroelectric phase-transition temperature. The existence of a very high value of NTE in the vicinity of the isostructural phase transition makes the study of this system very interesting. From Rietveld analysis of high resolution synchrotron x-ray powder diffraction (SXRD) (300 to 973 K) and laboratory x-ray powder diffraction (XRD) (13 to 300 K) data as a function of temperature in the range 13 to 973 K, we have calculated the change in atomic positions and the unit cell volume associated with this isostructural phase transition. Using group theoretical considerations we show that the observed atomic displacements at the isostructural phase-transition temperature can be described in terms of the displacement modes corresponding to one of the Irreps at the $\boldsymbol{k} = (0, 0, 0)$ point of the Brillouin zone of the *P*4*mm* space group. Based on the anomalies in the temperature dependence of the thermal displacement parameters as a function of temperature, we argue that the transition is most likely phonon driven, as against commonly known valence fluctuation[6–8] and magnetoelastic-coupling[14,15] driven isostructural phase transitions in metallic and multiferroic systems, respectively. We also locate a critical point in the *T*-*x* phase diagram of BF-*x*PT by studying the composition dependence of the T_1 to T_2 isostructural phase transition in the composition range $0.31 \leqslant x \leqslant 0.70$.

II. EXPERIMENTAL AND ANALYSIS

Samples of BF-*x*PT for $x = 0.31$, 0.40, 0.50, 0.60, and 0.70 were prepared by the solid-state thermochemical reaction route, using analytical reagent grade Bi_2O_3 (99.5%), Fe_2O_3 (99%), PbO (99%), and TiO_2 (99%) powders, details of which are reported elsewhere.[18] High temperature SXRD measurements were carried out at a wave length of 0.35 Å (35 keV) in the 300 to 973 K range at the BL02B2 beam line of SPring-8, Japan using a large Debye-Scherrer camera equipped with an imaging plate as a two-dimensional detector.[19] The temperature of the sample was varied using a hot N_2 gas-flow system with an accuracy of ±1 K. Low temperature XRD data in the 300 to 13 K range was collected on an 18-kW rotating anode-based powder x-ray diffractometer fitted with a He-close-cycle refrigerator-based low temperature attachment and a curved crystal monochromator in the diffraction beam. The temperature of the sample in the laboratory experiments was also controlled within ±1 K. Rietveld refinements of the powder diffraction data were carried out by FULLPROF[20] package. Irreducible atomic displacement modes were calculated using BasIreps software implemented in the FULLPROF package.

III. RESULTS AND DISCUSSION

A. Evidence for an intermediate phase in between the tetragonal and cubic phase fields

Figure 1(a) depicts the diffraction profiles of pseudocubic 100, 110, and 111 reflections of BF-0.31PT in the temperature range 13 to 973 K. It is evident from the figure that the 100 and 110 pseudocubic peaks are clearly split into 100, 001 and 110, 101 pair of reflections, while the 111 is a singlet in the entire temperature range 13 to 823 K. This is expected for the tetragonal structure. Thus there is no evidence of any structural change in the temperature range 13 to 823 K. New pairs of reflections, however, appear and coexist with those of the parent tetragonal phase, like the reflection pairs marked with asterisks in between the split 100 and 110 psuedocubic reflections of the parent tetragonal phase at 848 K [see Fig. 1(a)]. A new singlet 111 peak (marked with asterisk) near the original singlet 111 reflection has also appeared. All these indicate the onset of a structural phase transition around 848 K. With further increase in temperature of about 25 K, the reflections corresponding to the new phase become more intense than those of the parent tetragonal phase. On raising the temperature further to 898 K, the peaks corresponding to the parent tetragonal phase are found to be nearly absent. With further increase in temperature, splitting of the 100 and 110 pseudocubic reflections of the new phase decreases, and

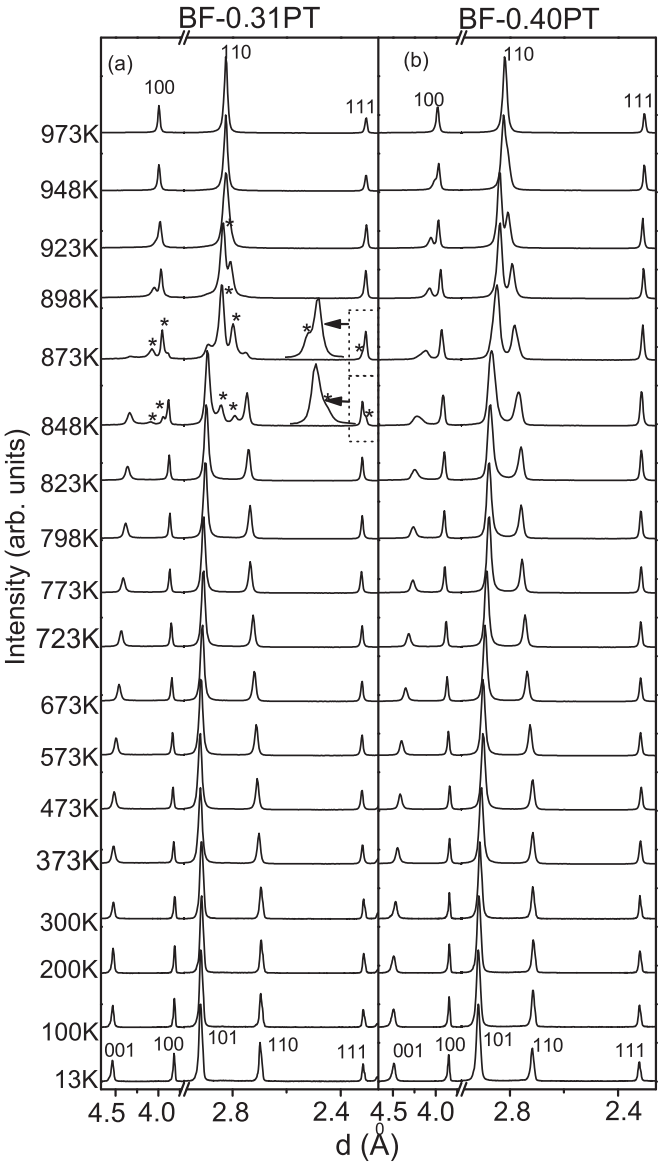

FIG. 1. Evolution of the profiles of 100, 110, and 111 pseudocubic reflections with temperature for (a) BF-0.31PT and (b) BF-0.40PT.

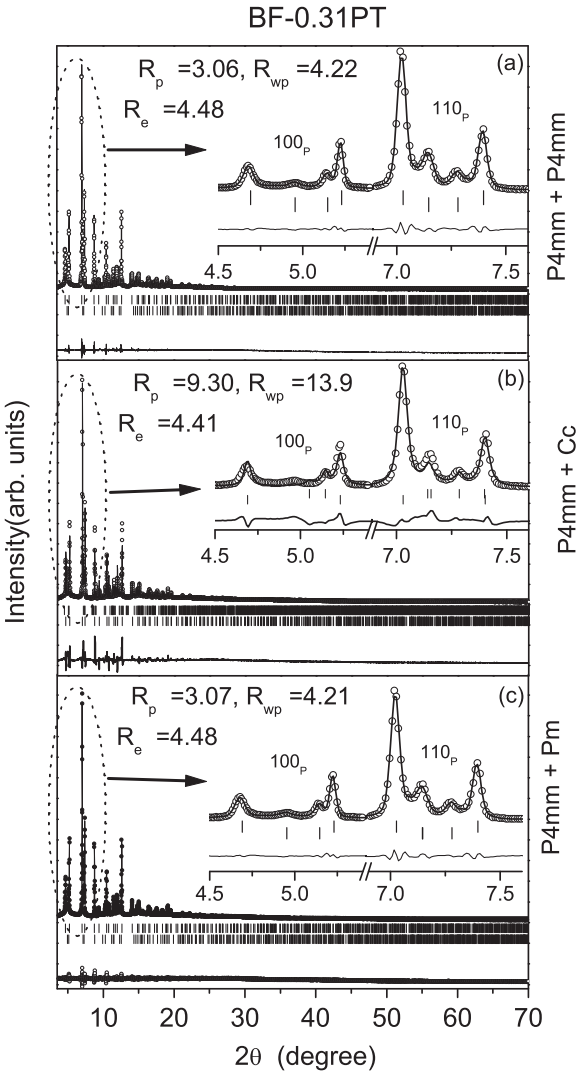

FIG. 2. Observed (dotted), calculated (continuous line), and difference profiles (bottom line) obtained from Rietveld analysis of powder-diffraction pattern of BF-0.31PT at 848 K using (a) two tetragonal phases (T_1 and T_2) both in the *P*4*mm* space group, (b) tetragonal *P*4*mm* (T_1) and monoclinic *Cc* space groups, and (c) tetragonal *P*4*mm* (T_1) and monoclinic *Pm* space groups.

the split peaks finally merge into one peak at 973 K when the structure becomes cubic. This gives ferroelectric-transition temperature as ∼973 K.

B. Structure of the intermediate phase

To identify the crystallographic symmetry of the new phase, Rietveld refinement was carried out using the diffraction data at various temperatures. As the pattern of the second phase resembles closely with the first tetragonal phase (which we shall henceforth call as T_1 phase), we first considered *P*4*mm* symmetry for the second phase (which shall be called as T_2 phase) also. In the tetragonal *P*4*mm* space group, Bi/Pb occupy 1a Wyckoff site (0, 0, *z*) and Fe/Ti occupy 1b Wyckoff site ($\frac{1}{2}$, $\frac{1}{2}$, *z*), whereas the oxygen atoms occupy two different sites [1b ($\frac{1}{2}$, $\frac{1}{2}$, *z*) and 2c ($\frac{1}{2}$, 0, *z*)]. The fit between the observed and calculated patterns obtained by Rietveld refinement for the model considering coexistence of T_1 and T_2 phases is shown in Fig. 2(a). It is evident from the quality of the fit that the model of two coexisting tetragonal phases explains very well the observed pattern. We also considered the monoclinic space group *Cc* for the second phase, proposed earlier on the basis of rotating anode data,[18] coexisting with the parent tetragonal phase in the *P*4*mm* space group. But the fit is rather poor [see Fig. 2(b)], ruling out the monoclinic *Cc* space group. The monoclinic space group *Cc* was proposed earlier on the presumption that the MPB is tilted towards the Ti-rich side.[18] But the present analysis with high resolution SXRD data shows that the situation is entirely different. In a recent work Ranjan and Raju[21] studied the stability of tetragonal phase of BF-*x*PT at high temperatures using low resolution laboratory XRD data. For $x = 0.35$, they studied the evolution of the tetragonal phase as a function of temperature and interpreted that the

parent tetragonal phase (room temperature phase) transforms into a lower symmetry monoclinic phase with *Pm* space group along with appearance of a new tetragonal phase. In support of this tetragonal to monoclinic transformation they have shown the appearance of a small hump on the left shoulder of the 110 tetragonal (parent low-temperature phase) reflection that cannot be accounted for by the tetragonal symmetry (see Fig. 3 of Ref. 21). But a perusal of the SXRD patterns for the 101 tetragonal reflection shown in Fig. 1 does not reveal any signature of a shoulder on the lower 2θ side of the 110 peak. Observation of a shoulder on the left arm of 110 tetragonal reflection by Ranjan and Raju is, therefore, an artifact of low resolution laboratory XRD data, or it could also be due to poor sample quality as evident from the extremely large width of the MPB region observed by them. Even in our earlier study on the evolution of the tetragonal phase (for $x = 0.31$) with temperature using rotating anode XRD data, we did not find this type of shoulder, although in that study the splitting of the 100 psuedocubic reflection of the second tetragonal phase (low tetragonality) was not clearly resolved, and due to that we interpreted it in terms of a monoclinic phase.[18] For both the *Cc* and *Pm* monoclinic space groups, the psuedocubic 111 peak should in principle be a triplet,[22] but usually two of these reflections are so close that this peak appears like a doublet. It is evident from Fig. 2 that neither the 111 peak of the parent phase nor that of the higher temperature phase is a triplet/doublet. It is indeed a nice singlet with resolution-limited width. All these observations reject the possibility of any phase transition from the parent tetragonal (T_1 phase) to a monoclinic phase in the *Pm* space group at high temperatures in BF-0.31PT. However the new phase (the T_2 phase), which appeared at 848 K, may possess symmetry lower than that of the tetragonal T_1 and hence has to be carefully examined. We therefore verified the absence of the monoclinic *Pm* space group (for T_2 phase) using Rietveld refinement. For this we considered coexistence of monoclinic phase in the *Pm* space group with tetragonal T_1 phase in *P*4*mm* space group in our refinements. In the *Pm* space group the 2c ($\frac{1}{2}$, 0, z) Wyckoff site of *P*4*mm* space group splits into 1a (x, 0, z) and 1b (x, $\frac{1}{2}$, z) Wyckoff sites, leading to altogether three different oxygen atoms in the asymmetric unit. It is found that the refined coordinates and lattice parameters of the *Pm* space group are equivalent to those of the tetragonal T_2 phase within the standard deviations, as can be seen from the values of refined parameters given in Table I. Our analysis thus comprehensively rejects the possibility of the monoclinic *Pm* space group. For the sake of completion we also give in Table I the refined parameters for the coexisting low temperature tetragonal phase (T_1).

C. Large volume collapse, NTE behavior and phase coexistence

Ferroelectric $PbTiO_3$ (PT) contracts with increase in temperature and shows a large bulk NTE with an expansion coefficient of $\overline{\alpha} = 1/V_o\ (\Delta V/\Delta T) = -1.99 \times 10^{-5}\ K^{-1}$ on approaching the ferroelectric phase-transition temperature.[23] The tetragonal phase of the solid solution system BF-xPT, stable in the composition range $x \geqslant 0.31$,[24] shows even larger NTE, and its value increases with increasing BF content towards the morphotropic phase boundary (MPB) region along with increase in tetragonality.[24–27] For $x = 0.40$ it shows

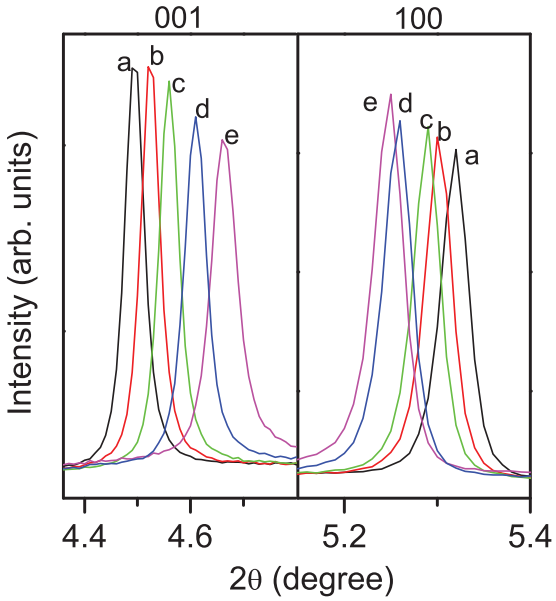

FIG. 3. (Color online) Evolution of 001 and 100 tetragonal reflections with temperature for BF-0.31PT. In this figure (a) to (e) correspond to temperatures 373, 573, 673, 773, and 823 K, respectively.

unusually large value of NTE with a bulk thermal-expansion coefficient $\overline{\alpha} \sim -3.92 \times 10^{-5}\ K^{-1}$.[26] But this composition does not correspond to the highest value of the tetragonality reported for BF-xPT.[24] The composition with $x = 0.31$ corresponds to the tetragonal phase closest to the MPB and shows higher tetragonality $\eta = c/a - 1 = 0.187$ than that for $x = 0.40$, which is merely $\eta = 0.170$.[22] This composition ($x = 0.31$) may therefore show even higher NTE coefficient.

The foregoing analysis in Sec. III B establishes beyond doubt that the room temperature tetragonal phase (T_1) in the *P*4*mm* space group with high tetragonality ($\eta = c/a - 1 = 0.187$ at 300 K) transforms to another tetragonal phase (T_2) in the same space group but with much lower tetragonality ($\eta = 0.041$ at 848 K) for BF-0.31PT. The NTE behavior of the T_1 phase is illustrated in Fig. 3, which compares the temperature evolution of the tetragonal 001 and 100 reflections for temperatures up to 823 K. From the figure it is evident that the unit cell parameter a ($= b$ in the tetragonal phase) expands normally as the 100 diffraction peak shifts towards lower 2θ value on higher temperatures, but the c parameter contracts with increase in temperature up to 823 K as the 001 peak shifts towards higher 2θ value. The variation of the unit cell parameters of BF-0.31PT (as obtained after Rietveld refinement of the XRD data in the temperature range 13 to 973 K) with temperature is shown in Fig. 4(a) while the variation of the unit cell volume is shown in Fig. 4(b). Temperature dependence of unit cell volume of the parent tetragonal phase (T_1) shows three different zones: first normal (positive) thermal expansion [PTE in Fig. 4(b)] behavior, followed by a nearly zero thermal expansion [ZTE in Fig. 4(b)] zone and then a large NTE [Fig. 4(b)] zone in the vicinity of the T_1 to T_2 phase transition. It is also evident from Fig. 4(b) that this transition is accompanied with a sharp collapse of volume (~2% at $T = 873$ K) at the T_1 to T_2 phase-transition temperature. This,

TABLE I. A comparison of the refined structural parameters of the low tetragonality tetragonal phase (T_2) in the *P*4*mm* space group and the recently proposed monoclinic phase in the *Pm* space group at 848 K. The structural parameters of the coexisting high tetragonality phase (T_1) are also given in the last column of this table. The refined parameters of the tetragonal T_2 phase and the monoclinic phase (*Pm*) are obviously equivalent.

Space group	*Pm* (M)	*P*4*mm* (T_2)	*P*4*mm* (T_1)
Lattice Parameters			
a (Å)	3.953(4)	3.953(3)	3.890(2)
b (Å)	3.952(4)	–	–
c (Å)	4.106(3)	4.107(7)	4.337(2)
β (°)	89.98(3)	90	90
Position coordinates			
Bi/Pb	fixed at (0,0,0)	fixed at (0,0,0)	fixed at (0,0,0)
Thermal parameter (Å^2)	$B_{iso} = 4.812(3)$	$B_{iso} = 4.810(4)$	$B_{iso} = 3.86(2)$
Fe/Ti			
x	0.500(3)	0.5	0.5
y	0.5	0.5	0.5
z	0.576(6)	0.576(7)	0.563(4)
Thermal parameter (Å^2)	$B_{iso} = 2.391(3)$	$B_{iso} = 2.389(6)$	$B_{iso} = 1.73(3)$
O1			
x	0.499(6)	0.5	0.5
y	0.5	0.5	0.5
z	0.009(6)	0.012(3)	0.161(6)
Thermal parameter (Å^2)	$B_{iso} = 3.55(2)$	$B_{iso} = 3.56(6)$	$\beta_{11} = 0.070(1)$ $\beta_{22} = 0.070(1)$ $\beta_{33} = 0.060(5)$
O2			
x	−0.001(2)	0.0	0.0
y	0.5	0.5	0.5
z	0.498(6)	0.504(9)	0.637(7)
Thermal parameter (Å^2)	$B_{iso} = 1.670(3)$	$B_{iso} = 1.665(4)$	$B_{iso} = 1.814(1)$
O3			
x	0.501(2)	0.5	0.5
y	0.0	0.0	0.0
z	0.497(4)	0.504(9)	0.637(7)
Thermal parameter (Å^2)	$B_{iso} = 1.670$ (3)	$B_{iso} = 1.665(4)$	$B_{iso} = 1.814(1)$
R_p, R_{wp}, R_e (%)	3.07, 4.21, 4.48 [T_1 + M]	3.06, 4.22, 4.48 [T_1 + T_2]	
χ^2	0.90	0.885	

along with the fact that the two tetragonal phases coexist in the 848 to 898 K temperature range (see Fig. 1), show the first-order character of the T_1 to T_2 transition. The gradual transformation of the parent tetragonal phase (T_1) is illustrated in terms of its phase fraction in the inset of Fig. 4(b). At 848 K, ∼30% of the parent phase gets transformed into the new phase (T_2), whereas this value increases to 70% and 92% at 873 K and 898 K, respectively. The bulk average thermal expansion coefficient $\overline{\alpha}$ for the parent tetragonal phase (T_1) in the temperature range 673 to 848 K is -4.69×10^{-5} K^{-1}, which is higher than the highest value reported for BF-xPT with $x = 0.4$ in the literature.[26]

At 923 K, the high tetragonality phase (T_1) disappears, but the low tetragonality phase (T_2) is found to coexist with the cubic phase. This was confirmed by Rietveld refinements using the data at 923 K. This phase coexistence suggests that the transformation from the second tetragonal phase (T_2) to the paraelectric cubic (C) phase is also a first-order phase transition. Further, the T_2 phase also exhibits NTE behavior, as can be seen from Fig. 4(b).

D. Symmetry mode analysis of the T_1 to T_2 isostructural phase transition

The tetragonal T_1 to tetragonal T_2 phase transition of BF-0.31PT is an isostructural phase transition involving preservation of both the space group symmetry and the type of occupied Wyckoff positions. It is obviously not governed by valence fluctuations. In order to get insight into the mechanism of this transition, we analyzed the evolution of the atomic displacements with temperature across the isostructural phase-transition temperature. Displacement (in Å) along z direction for Fe/Ti, O1, and O2 were calculated with respect to their undistorted (cubic) position. Although only the z coordinates of Ti/Fe and O atoms are refined in the *P*4*mm* space group, the x and y displacements of O1, O2, and Fe/Ti atoms also change

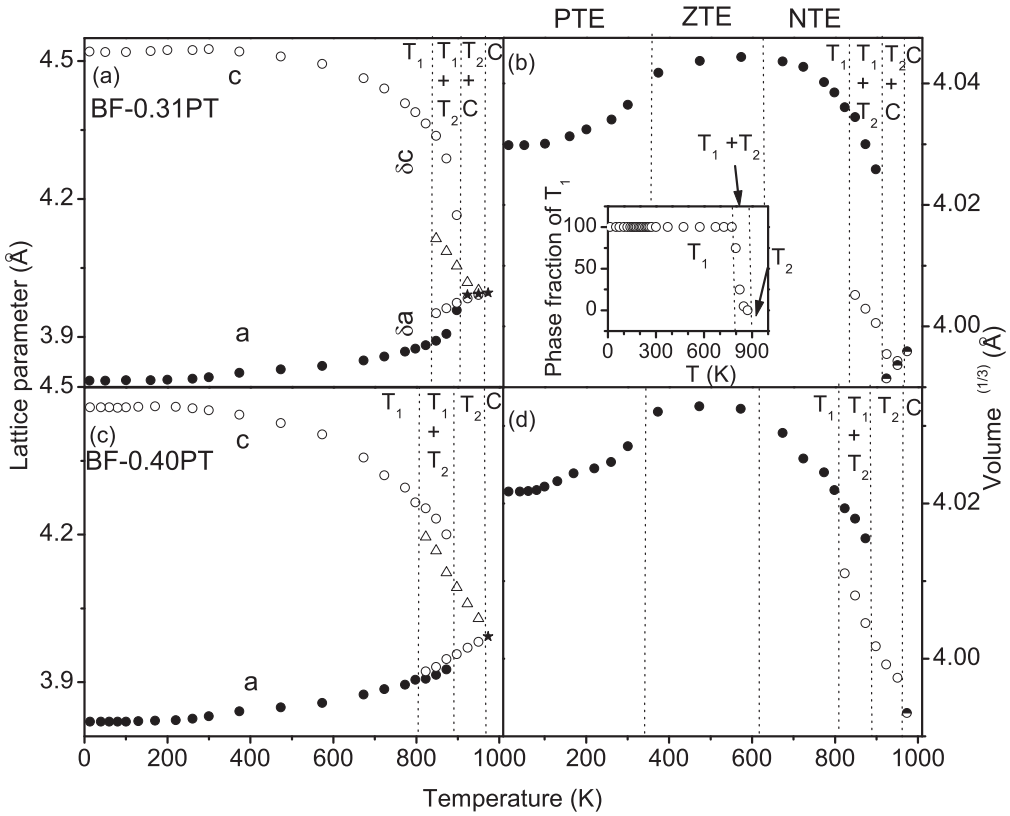

FIG. 4. Variation of lattice parameters of the tetragonal (T_1 and T_2) and cubic (C) phases with temperature obtained from Rietveld refinement for (a) BF-0.31PT and (c) BF-0.40PT. Variation of unit cell volume of the tetragonal (T_1 and T_2) and cubic (C) phases with temperature for (b) BF-0.31PT and (d) BF-0.40PT. PTE, ZTE, and NTE correspond to positive thermal expansion, nearly zero thermal expansion, and NTE, respectively.

because of the temperature variation of the a and b lattice parameters. The evolution of the atomic displacements of constituent atoms in the asymmetric unit of the two tetragonal ($P4mm$) phases with temperature is shown in Fig. 5. The abrupt shift in the atomic positions at the tetragonal (T_1) to tetragonal (T_2) phase-transition temperature is clearly seen in Fig. 5. We now proceed to analyze these shifts in the atomic positions using group theoretical treatment to see the possible role of phonon modes in causing these displacements.

Because the translational symmetry is not lost in this transition, the order parameter inducing this structural transition must belong to the zone center. There are, in general, five Irreps of the $P4mm$ space group at $\boldsymbol{k} = (0, 0, 0)$. Table II shows the character of each symmetry element of the five Irreps (IRs) at $\boldsymbol{k} = (0, 0, 0)$ as obtained from BasIreps software of FULLPROF package.[20] Out of these five, only IR(1), IR(3), and IR(5) are active for the $P4mm$ space group of the ABO_3 type perovskite structure. Atomic displacements associated with the various Wyckoff sites of the $P4mm$ space group of perovskites can be decomposed into contributions from different modes with symmetries given by the following Irreps[20]:

$$\Gamma_{1(a)} = \mathrm{IR}(1) + \mathrm{IR}(5);\ \Gamma_{1(b)} = \mathrm{IR}(1) + \mathrm{IR}(5);$$
$$\Gamma_{2(c)} = \mathrm{IR}(1) + \mathrm{IR}(3) + 2\mathrm{IR}(5).$$

The nature of atomic displacement due to a particular phonon mode can be described by its symmetry adopted basis vectors. In general the displacement of atom j in cell L may be written as a Fourier series of the form[20]

$$\boldsymbol{D}_{jL} = \Sigma \boldsymbol{u}_{kj} \exp(-2\pi i \boldsymbol{k} \cdot \boldsymbol{R}_L),$$

where $\boldsymbol{k}$ and $\boldsymbol{R}_L$ are vectors referring to the reciprocal and direct crystallographic basis, respectively. The vectors $\boldsymbol{u}_{kj}$ are the Fourier components of the displacements $\boldsymbol{D}_{jL}$ and

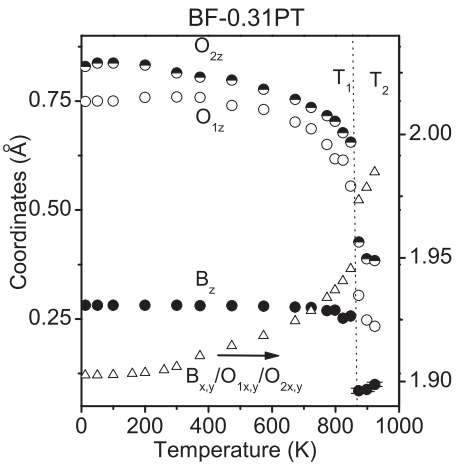

FIG. 5. Variation of positional coordinates (in Å) of Fe/Ti (B) and oxygen atoms (O1 and O2) in the tetragonal ($P4mm$) unit cell with temperature across the isostructural phase transition temperature for BF-0.31PT.

TABLE II. Character table of the five possible Irreps of *P*4*mm* space group at $\boldsymbol{k} = (0,0,0)$.

Irreducible representation	Symmetry elements (Kovalev)							
	{1|000}	{2_00*z*|000}	{4+_00*z*|000}	{4-_00*z*|000}	{m_*x*0*z*|000}	{m_0*yz*|000}	{m_*x*-*xz*|000}	{m_*xxz*|000}
IR(1)	1	1	1	1	1	1	1	1
IR(2)	1	1	1	1	−1	−1	−1	−1
IR(3)	1	1	−1	−1	1	1	−1	−1
IR(4)	1	1	−1	−1	−1	−1	1	1
IR(5)	1 0 0 1	−1 0 0 −1	i 0 0 −i	−i 0 0 i	0 1 1 0	0 −1 1 0	0 −i i 0	0 i −i 0

are referred to as basis of unit vectors along the direct crystallographic cell basis. Taking into account the symmetry, the vectors $\boldsymbol{u}_{\boldsymbol{k}j}$ may be written as linear combinations of the so-called basis functions of the Irreps of the propagation vector group $G_{\boldsymbol{k}}$.

The basis vectors (non-normalized) representing the displacement modes for each Wyckoff site of the tetragonal *P*4*mm* phase of perovskites are shown in Table III. On transforming from T_1 to T_2 phase, both the x (=y) and z components (in Å) of the atomic positions (with respect to the Bi/Pb at the origin) in the unit cell get significantly changed. A comparison of the atomic displacements across the T_1 to T_2 phase transition shown in Fig. 5 with those predicted theoretically in Table III shows that the observed displacements can be explained by the symmetry-adapted basis vectors of two different Irreps, IR(1) (in z direction) and IR(5) (in the *ab* plane) of the tetragonal *P*4*mm* phase of the ABO_3 structure. IR(3) cannot explain the displacement of Bi/Pb and Fe/Ti atoms. The space group symmetry and the symmetry-adapted strain induced by order parameters corresponding to the individual Irreps are shown in Table IV. It is evident from Table II that IR(1) is a symmetry preserving Irrep, but IR(5) is not. So, involvement of IR(5) Irrep will reduce the space group symmetry and hence any change in atomic position and lattice parameters that takes place through this transition has to be explained by the IR(1) alone. In order to explain the shifts of positions of atoms in the *xy* plane, the strain field associated with IR(1) Irrep has to be considered in this transition. Thus the group theoretical analysis of the observed displacement patterns shown in Fig. 6 confirms that an isostructural phase transition from one tetragonal phase (T_1) with high tetragonality to another (T_2) with lower tetragonality can occur through the condensation of the symmetry preserving IR(1) mode of the *P*4*mm* space group.

E. Possible role of phonons in the T_1 to T_2 isostructural phase transition

In order to provide additional evidence for the role of phonon modes in the T_1 to T_2 isostructural phase transition, mean-square isotropic atomic displacement parameters of the atoms in the unit cell have been analyzed in the temperature range from 13 to 973 K for BF-0.31PT. The variation of displacement parameters around a particular phase transition can give valuable information about the involvement of phonons in that transition. Any deviation from the normal trend (i.e., the nature expected from Debye Waller-type expansion) around a structural phase transition gives direct signature of the involvement of phonons in the transition. Figure 6 depicts the variation of the mean-square isotropic atomic displacement parameters with temperature for various atoms in the asymmetric unit of T_1, T_2, and C phases. Displacement parameter of Bi/Pb shows clear deviation around the two transitions, first for C to T_2 transition and second

TABLE III. Basis vectors (mechanical) of the three active Irreps of *P*4*mm* space group of ABO_3 at $\boldsymbol{k} = (0, 0, 0)$ at various Wyckoff sites.

Irreducible representation	Basis vector		1a site (0, 0, *z*)	1b site ($\frac{1}{2}$, $\frac{1}{2}$, *z*)	2c site ($\frac{1}{2}$, 0, *z*) (0, $\frac{1}{2}$, *z*)
IR(1)	$\tau_{1,1}$	Re	(0 0 1)	(0 0 1)	(0 0 1) (0 0 1)
		Im			
IR(3)	$\tau_{3,1}$	Re			(0 0 1) (0 0 -1)
		Im			
IR(5)	$\tau_{5,1}$	Re	(1 0 0)	(1 0 0)	(1 0 0) (0 0 0)
		Im	(0 -1 0)	(0 -1 0)	(0 0 0) (0 -1 0)
	$\tau_{5,2}$	Re	(1 0 0)	(1 0 0)	(0 1 0) (0 0 0)
		Im	(0 1 0)	(0 1 0)	(0 0 0) (1 0 0)
	$\tau_{5,3}$	Re			(1 0 0) (0 0 0)
		Im			(0 0 0) (0 1 0)
	$\tau_{5,4}$	Re			(0 -1 0) (0 0 0)
		Im			(0 0 0) (1 0 0)

TABLE IV. Reduced-space groups corresponding to each Irreps at the zone center of *P*4*mm* space group. Associated symmetry adapted strains are also shown.

Irreducible representation	Reduced-space group	Strain
IR(1)	*P*4*mm*	$e_{xx} + e_{yy}, e_{zz}$
IR(2)	*Pmm*2	$e_{xx} - e_{yy}$
IR(3)	*Cmm*2	e_{xy}
IR(4)	*P*4	none
IR(5)	*Pm*, *Cm*, P1	e_{xz}, e_{yz}

for isostructural transition from T_2 to T_1. The mean-square atomic displacement parameter gets reduced by a significant amount ($\sim$0.01 Å^2) upon transition into the tetragonal T_2 phase from the nonpolar C phase. The displacement parameter of Bi/Pb is reduced further and discontinuously at the T_2 to T_1 phase-transition temperature. The displacement parameter for Fe/Ti also shows a clear discontinuity at the isostructural phase-transition temperature. The displacement parameter of Fe/Ti gets reduced by $\sim$0.008 Å^2 after transforming into the T_1 phase from the T_2 phase but there is much smaller difference in the displacement parameters of Fe/Ti in the cubic and T_2 phases. After transition into the T_1 phase, the displacement parameters show the same trend down to very low temperatures ($\sim$13 K) without showing any further anomalous nature.

It is well known that Γ_4^- phonon of the cubic phase gets frozen at the cubic-to-tetragonal ferroelectric phase transition in ABO_3 perovskites. The reduction of displacement parameters upon transforming into tetragonal (T_2) phase from the cubic phase clearly shows the signature of this phonon condensation. The anomalous nature shown by the mean-square atomic displacement parameters across the isostructural T_2 to T_1 transition in the same way, signifies the role played by the phonons. The displacement parameters of Bi/Pb and Fe/Ti do not approach zero value with the temperature approaching absolute zero (Fig. 6), showing that significant amount of disorder is present for these two atomic sites.

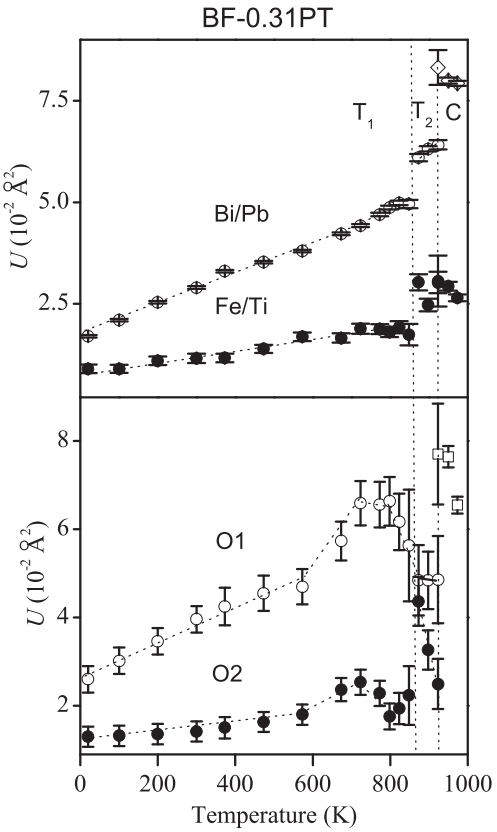

FIG. 6. Variation of mean-square atomic displacement parameters U (Å^2) of Bi/Pb, Fe/Ti, and oxygen atoms (O1 and O2) with temperature in the range 13 to 973 K.

Extracting meaningful mean-square atomic-displacement parameters for lighter atoms such as oxygen from x-ray diffraction at elevated temperatures is always a challenge, but with the help of high resolution and high energy (35 keV) SXRD data, such as that used in the present work from SPring-8, containing high-order reflections at very high 'q' values, one can obtain reliable values of the displacement parameters. The evolution of the displacement parameters of oxygen atoms from 13 to 973 K is shown in Fig. 6. As can be seen from the figure, O2 shows clear anomaly at both the transitions. After transition into the T_2 phase from cubic phase, a drop of $\sim$0.05 Å^2 is observed in the displacement parameter of O2, indicating clear signature of phonon condensation. The displacement parameter of O2 in the T_2 phase shows increasing nature as the temperature decreases and approaches the isostructural phase-transition temperature. Upon transformation into the T_1 phase, it shows a discontinuous change followed by an initial saturation and subsequent slow decrease with temperature. The displacement parameter of O1 shows a similar condensation upon transforming into the T_2 phase from the cubic phase and gets reduced by $\sim$0.03 Å^2. It remains nearly constant in the T_2 phase, but upon transforming into the T_1 phase its value gets a little increased, followed by saturation and subsequent gradual decrease in the T_1 phase just after the transition. The anomalous nature of atomic displacement parameters points towards the involvement of phonons in this transition. Raman and IR studies are required to further confirm the role of phonons in the isostructural phase transition of BF-xPT.

F. Composition dependence of the isostructural phase transition and location of a critical point in the phase diagram of BF-xPT

PT forms a continuous solid solution with BF and shows an MPB, separating the stability fields of tetragonal and monoclinic phases[18,24,25] similar to that observed in the technologically important piezoelectric MPB systems such as $PbZrO_3$-$x$$PbTiO_3$ (PZT), $Pb(Mg_{1/3}Nb_{2/3})O_3$-$x$$PbTiO_3$ (PMN-PT), $Pb(Zn_{1/3}Nb_{2/3})O_3$-$x$$PbTiO_3$ (PZN-PT), etc. (see the reviews by Noheda *et al.* and Pandey *et al.*[29]). The MPB in the PZT, PMN-PT, and PZN-PT, etc., is known to be slightly tilted towards the Ti-deficient side in the monoclinic/pseudo-rhombohedral phase region as the temperature approaches the ferroelectric-transition temperature (T_C). In a previous report[18] it was proposed that the MPB in BF-xPT system is tilted toward the Ti-rich tetragonal side. Due to the limited resolution of the rotating anode XRD data, it was concluded that the room temperature tetragonal phase for $x = 0.31$ transforms to a monoclinic phase at high temperatures. With the high resolution SXRD data for $x = 0.31$, we have now identified

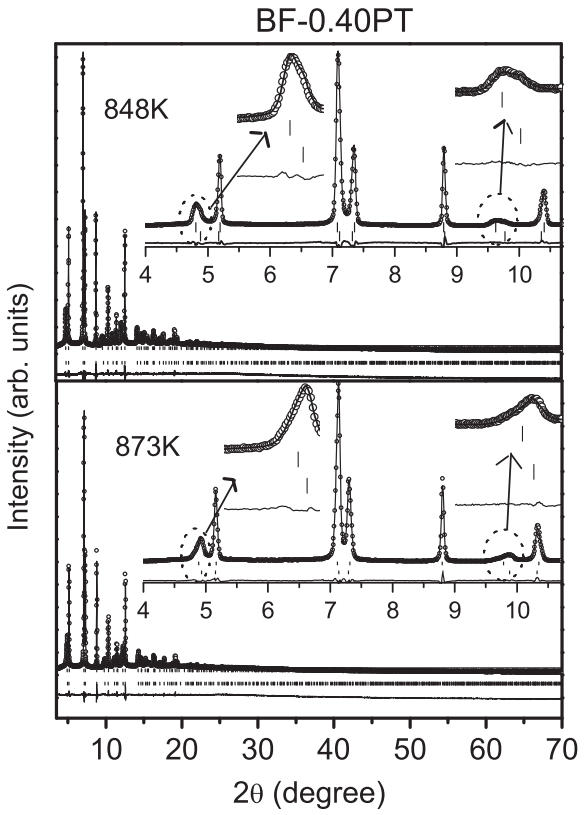

FIG. 7. Observed (dotted), calculated (continuous line), and difference patterns (bottom line) obtained from Rietveld analysis of powder-diffraction profile of BF-0.40PT using two tetragonal phases (both in the *P*4*mm* space group) at $T = 848$ K (upper panel) and at 873 K (lower panel).

the true symmetry of the higher temperature phase, which is also tetragonal. In our previous work[18] we presented a phase diagram of BF-*x*PT. In the light of the discovery of the T_1 to T_2 isostructural phase transition described in the present work, the phase diagram proposed in Ref. 18 needs modification. For this we have investigated the composition dependence of the T_1 to T_2 isostructural phase transition in BF-*x*PT system for the range $0.31 \leqslant x \leqslant 0.70$. This study acquires special significance as the existence of an isostructural phase transition in the temperature vs composition (x) phase diagram (T-x) should enable us to locate a critical point in the BF-*x*PT phase diagram. A critical point should exist between the stability region of T_1 and T_2 phases since they do not differ in the internal symmetry (see, for definition of critical point, Ref. 3).

Our investigations on the BF-*x*PT compositions with $x > 0.31$ reveal that the signature of T_1 to T_2 transition becomes increasingly more subtle on increasing the PT content (x). To illustrate this, we depict in Fig. 1(b) the evolution of XRD profiles of 100, 110, and 111 pseudocubic reflections of BF-0.40PT as a function of temperature in the range 13 to 973 K. As in the case of BF-0.31PT, the tetragonal splitting of the perovskite 100 and 110 peaks of BF-0.40PT decreases with an increase in temperature. However, unlike BF-0.31PT, the appearance of the peaks corresponding to the second phase is not clearly visible in the high temperature profiles of BF-0.40PT. However, a careful examination of the profile of the 001 reflection reveals an increasingly large asymmetric

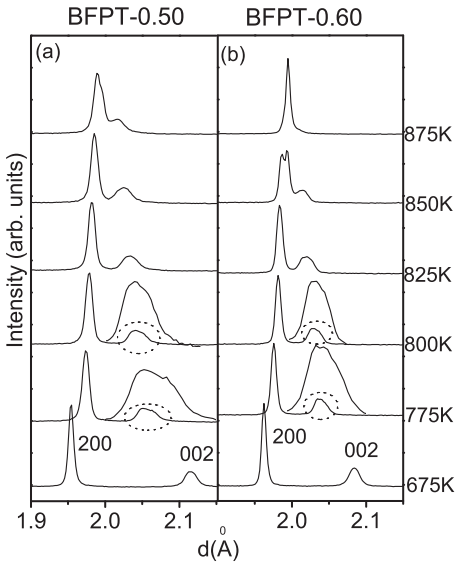

FIG. 8. Evolution of 200, 002 pseudocubic reflections with temperature in the vicinity of the isostructural phase transition for (a) BF-0.50PT and (b) BF-0.60PT. The 002 profile is further zoomed in the 775 and 800 K patterns.

broadening on the high 2θ side in the temperature range 798 to 848 K, suggesting the appearance of another peak in the tail of the 001 reflection. On increasing the temperature from 848 to 873 K, the intensity of the new reflection increases while that of the parent 001 peak decreases as a result of which the asymmetric broadening of the 001 peak now occurs on the lower 2θ side rather than on the higher 2θ side for 798 K $\leqslant T \leqslant$ 848 K. With further increase in temperature to 898 K, the asymmetric broadening decreases drastically, revealing the decrease in the phase fraction of the parent tetragonal phase. At around $T = 923$ K, this asymmetry nearly disappears leaving behind the peaks of the second phase only. At ~973 K, all splittings disappear, and the structure becomes cubic. That the asymmetry broadening in the temperature range 823 to 898 K is due to the coexistence of T_1 and T_2 phases was confirmed by Rietveld refinements. Figure 7 depicts the results of Rietveld refinements at $T = 848$ and 873 K. The excellent fit between the observed and calculated profiles, especially for the asymmetrically broadened reflections like 001 and 002 shown in the inset to Fig. 7, not only confirms the coexistence of the T_1 and T_2 phases in the temperature range 823 to 898 K but also reveals that the phase fraction of the T_1 phase decreases while that of T_2 increases on increasing the temperature. We can thus conclude that BF-0.40PT also undergoes T_1 to T_2 isostructural phase transition. The variation of the unit cell parameters and the unit cell volume of BF-0.40PT with temperature is depicted in Figs. 4(c) and 4(d), respectively. The variations are similar to those for BF-0.31PT showing NTE, ZTE, and PTE behaviors with decreasing temperature but with one important difference: The volume change (ΔV) at the T_1 to T_2 transition is reduced by a factor of 1/5 for BF-0.40PT, as compared to that for BF-0.31PT.

We have observed subtle signatures of T_1 to T_2 transition for $x = 0.5$ and 0.6 also. To illustrate this, we depict in Fig. 8 the diffraction profiles of 200 and 002 tetragonal reflections in the temperature range 675 to 875 K for both the compositions.

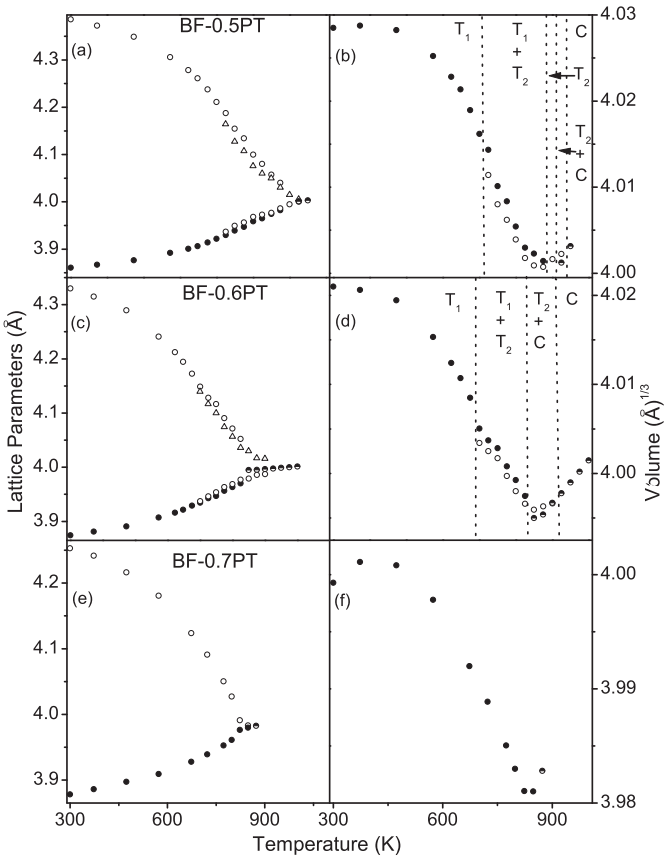

FIG. 9. Variation of lattice parameters of the tetragonal (T_1 and T_2) and cubic (C) phases with temperature obtained from Rietveld refinement for (a) BF-0.50PT, (c) BF-0.60PT, and (e) BF-0.7PT. Variation of unit cell volume of the tetragonal (T_1 and T_2) and cubic (C) phases with temperature for (b) BF-0.50PT, (d) BF-0.60PT, and (f) BF-0.70PT. For BF-0.70PT the T_1 phase transforms directly into the cubic phase.

At 675 K the structure is tetragonal (T_1 phase) for both the compositions. Diffraction patterns at temperatures $T = 775$, 800, and 825 K show clear signature of T_1 and T_2 phase coexistence. The tetragonal 002 reflection is not a singlet in this temperature range. For BF-0.50PT, phase coexistence of the two tetragonal phases exists up to 875 K, whereas for BF-0.60PT the T_2 phase coexists with the cubic phase at 850 K and 875 K. All these were confirmed by Rietveld refinements. The variation of the unit cell parameters and unit cell volume with temperature for BF-0.50PT and BF-0.60PT is shown in Figs. 9(a)–9(d). It is evident from this figure that volume change at the T_1 to T_2 phase transition decreases on increasing the PT content from $x = 0.40$ to 0.60. For BF-0.70PT, we observe direct transition from the room temperature T_1 phase to the high temperature paraelectric-cubic phase without the intermediate T_2 phase observed for $0.31 \leqslant x \leqslant 0.60$. The variation of the volume change (ΔV) at the T_1 to T_2 phase transition as a function of PT content (x) is depicted in Fig. 10. It is evident that for $x \approx 0.63$, the volume difference, and hence the density difference, between the T_1 and T_2 phases disappears. This composition $x \approx 0.63$ thus corresponds to the critical point in the phase diagram of BF-xPT. It is interesting to note that with increasing PT content (x), the temperature

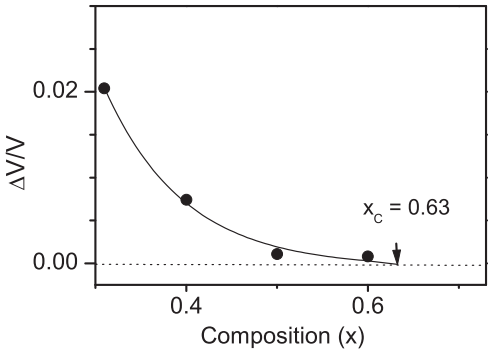

FIG. 10. Variation of the discontinuous change in the unit cell volume (ΔV) of BF-xPT at the T_1 to T_2 phase transition with composition (x). ΔV vanishes at $x = 0.63$ corresponding to a critical point in the phase diagram.

range of T_1 and T_2 phase coexistence increases. Further, for $0.50 \leqslant x \leqslant 0.60$, the NTE region extends nearly up to 450 K, whereas it extends up to ~400 K for $x = 0.70$.

Figure 11 depicts the modified-phase diagram of the BF-xPT system showing the phase boundary between the T_1 and T_2 phases and also the critical point marked with a 'cross' at $T \sim 677$ K for $x = 0.63$. For the sake of completeness, we have also plotted the magnetic-transition temperatures in Fig. 11 using data given in Refs. 30 and 31. The phase diagram of the BF-xPT system is evidently far richer than the phase diagram of other MPB systems such as PZT, PMN-xPT, and PZN-xPT in the sense that it not only shows magnetic-phase boundaries and disappearance of the tilted octahedral structure at the MPB for $x \geqslant 0.31$ but also contains a critical point at $x \sim 0.63$ away from the MPB.

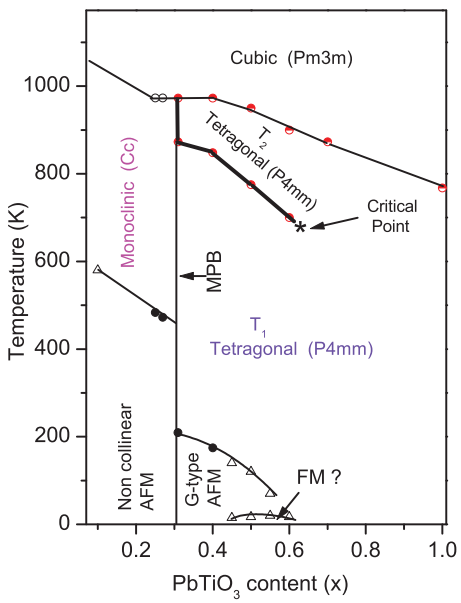

FIG. 11. (Color online) Phase diagram of BF-xPT in the vicinity of the MPB. The critical point occurs at $T = 677$ K and $x = 0.63$. All phase boundaries ($Cc/Pm\bar{3}m$), $P4mm(T_2)/Pm\bar{3}m$, $P4mm(T_1)/P4mm(T_2)$, and $P4mm(T_1)/Pm\bar{3}m$ are first order and have a coexistence region. The data points marked with -°-, -●- (black), and Δ are from Refs. 18, 30, and 31, respectively. AFM and FM stand for antiferromagnetic and ferromagnetic phases, respectively.

IV. SUMMARY

To summarize, we have investigated the high temperature phase transitions in the tetragonal phase of $(1–x)BiFeO_3$-$xPbTiO_3$ system for the composition range $0.31 \leqslant x \leqslant 0.70$. For the composition $x = 0.31$ (BF-0.31PT) that is closest to the MPB showing unusually large tetragonality, the room temperature tetragonal phase (T_1) undergoes an isostructural phase transition to another tetragonal phase (T_2) with much lower tetragonality without losing the space group symmetry just below the ferroelectric to paraelectric phase-transition temperature. This isostructural phase transition is accompanied with a large collapse of unit cell volume. The atomic displacements associated with this transition correspond to one of the irreducible representations of the *P4mm* space group associated with a phonon mode at the Brillouin zone center. The observation of strong anomalies in the thermal displacement parameters at the T_1 to T_2 isostructural phase-transition temperature suggests that this transition may be phonon driven as against the well-known valence fluctuation or magnetoelastic-coupling driven isostructural phase transitions. This is the first experimental observation of an isostructural phase transition involving two ferroelectric phases in a displacive ferroelectric system. From a study of the composition dependence of this isostructural phase transition in the range $0.31 \leqslant x \leqslant 0.70$, the existence of a critical point in the T-x phase diagram of BF-xPT system at $T \sim 677$ K for $x = 0.63$ has been confirmed. A complete phase diagram showing the boundaries between various crystallographic and magnetic phases has been established.

ACKNOWLEDGMENTS

D.P. and Y.K. acknowledge support from DST, Govt. of India, and JSPS of Japan under the Indo-Japan Science Collaboration Program. S. Bhattacharjee acknowledges the award of Senior Research Fellowship of CSIR, India. The synchrotron radiation experiments were performed at the BL02B2 of SPring-8 with the approval of the Japan Synchrotron Radiation Research Institute (JASRI) (Proposal No. 2010B0084).

*dpandey_bhu@yahoo.co.in

[1] J. C. Toledano and P. Toledano, *The Landau Theory of Phase Transitions* (World Scientific Publishing Co. Pte. Ltd., Singapore, 1987).

[2] P. Toledano and V. Dmitriev, *Reconstructive Phase Transitions: In Crystals and Quasicrystals* (World Scientific Publishing Co. Pte. Ltd., Singapore, 1996), Chaps. I and II.

[3] P. M. Chaikin and T. C. Lubensky, *Principles of Condensed Matter Physics* (Cambridge University Press, Cambridge, UK, 1995), p. 4.

[4] P. W. Anderson, *Basic Notions of Condensed Matter Physics* (The Benjamin/Cummings Publishing Company, Inc., Menlo Park, California, 1984), Chap. 2.

[5] J. F. Scott, Adv. Mater. **22**, 2106 (2010).

[6] A. Jayaraman, Phys. Rev. **139**, A690 (1965).

[7] M. K. Wilkinson, H. R. Child, C. J. Mchargue, W. C. Koehler, and E. O. Wollan, Phys. Rev. **122**, 1409 (1961).

[8] A. Jayaraman, A. K. Singh, A. Chatterjee, and S. Usha Devi, Phys. Rev. B **9**, 2513 (1974).

[9] L. Z. Liu, J. W. Allen, O. Gunnarsson, N. E. Christensen, and O. K. Andersen, Phys. Rev. B **45**, 8934 (1992).

[10] A. Solontsov and A. Mirmelstein, Phys. Lett. A **372**, 2086 (2008).

[11] S. Banerjee, D. Nath, and B. K. Chaudhuri, Phys. Rev. B **25**, 1883 (1982).

[12] H. Kiriyama, K. Kitahama, O. Nakamura, and R. Kiriyama, Bull. Chem. Soc. Jpn. **46**, 1389 (1973).

[13] S. Greenwald and J. S. Smart, Nature **167**, 364 (1951).

[14] S. Lee, A. Pirogov, M. Kang, K.-H. Jang, M. Yonemura, T. Kamiyama, S.-W. Cheong, F. Gozzo, N. Shin, H. Kimura, Y. Noda, and J.-G. Park, Nature **451**, 805 (2008).

[15] A. Singh, V. Pandey, R. K. Kotnala, and D. Pandey, Phys. Rev. Lett. **101**, 247602 (2008).

[16] H. Moriwake, Y. Koyama, K. Matsunaga, T. Hirayama, and I. Tanaka, J. Phys. Cond. Matt. **20**, 345207 (2008); S. Tinte, K. M. Rabe, and D. Vanderbilt, Phys. Rev. B **68**, 144105 (2003).

[17] A. J. Hatt, N. A. Spaldin, and C. Ederer, Phys. Rev. B **81**, 054109 (2010); R. J. Zeches, M. D. Rossell, J. X. Zhang, A. J. Hatt, Q. He, C.-H. Yang, A. Kumar, C. H. Wang, A. Melville, C. Adamo, G. Sheng, Y.-H. Chu, J.-F. Ihlefeld, R. Erni, C. Ederer, V. Gopalan, L. Q. Chen, D. G. Schlom, N. A. Spaldin, L. W. Martin, and R. Ramesh, Science **326**, 977 (2009); H. M. Christen, J. H. Nam, H. S. Kim, A. J. Hatt, and N. A. Spaldin, Phys. Rev. B **83**, 144107 (2011).

[18] S. Bhattacharjee and D. Pandey, J. Appl. Phys. **107**, 124112 (2010).

[19] E. Nishibori, M. Takata, K. Kato, M. Sakata, Y. Kubota, S. Aoyagi, Y. Kuroiwa, M. Yamakata, and N. Ikeda, Nucl. Instrum. Methods Phys. Res. A **467-468**, 1045 (2001).

[20] J. Rodríguez-Carvajal, FULLPROF, a Rietveld and pattern matching analysis program, Laboratoire Léon Brillouin (CEA-CNRS), France [http://www.ill.eu/sites/fullprof/].

[21] R. Ranjan and K. A. Raju, Phys. Rev. B **82**, 054119 (2010).

[22] Ragini, S. K. Mishra, D. Pandey, H. Lemmens, and G. Van Tendeloo, Phys. Rev. B **64**, 054101 (2001); D. M. Hatch, H. T. Stokes, R. Ranjan, Ragini, S. K. Mishra, D. Pandey, and B. J. Kennedy, *ibid.* **65**, 212101 (2002); A. K. Singh and D. Pandey, *ibid.* **67**, 064102 (2003).

[23] G. Shirane, S. Hoshino, and K. Suzuki, Phys. Rev. **8**, 1105 (1950).

[24] S. Bhattacharjee, S. Tripathi, and D. Pandey, Appl. Phys. Lett. **91**, 042903 (2007).

[25] R. T. Smith, G. D. Achenbach, R. Gerson, and W. J. James, J. Appl. Phys. **39**, 70 (1968).

[26] J. Chen, X. R. Xing, G. R. Liu, J. H. Li, and Y. T. Liu, Appl. Phys. Lett. **89**, 101914 (2006).

[27] V. V. S. S. Sai Sunder, A. Halliyal, and A. M. Umarji, J. Mater. Res. **10**, 1301 (1995).

[28] S. Bhattacharjee, V. Pandey, R. K. Kotnala, and D. Pandey, Appl. Phys. Lett. **94**, 012906 (2009).

[29] B. Noheda and D. E. Cox, Phase Transitions **79**, 5 (2006); D. Pandey, A. K. Singh, and S. Baik, Acta Crystallogr. A **64**, 192 (2008).

[30] S. Bhattacharjee, A. Senyshyn, P. S. R. Krishna, H. Fuess, and D. Pandey, Appl. Phys. Lett. **97**, 262506 (2010).

[31] W.-M. Zhu, H.-Y. Guo, and Z.-G. Ye, Phys. Rev. **78**, 014401 (2008).